Han, X., Franssen, H-J. H., Bello, M. Á. J., Rosolem, R., Bogena, H., Alzamora, F. M., Chanzy, A., & Vereecken, H. (2016). Simultaneous soil moisture and properties estimation for a drip irrigated field by assimilating cosmic-ray neutron intensity. *Journal of Hydrology*, *539*, 611-624. https://doi.org/10.1016/j.jhydrol.2016.05.050

Simultaneous Soil Moisture and Properties Estimation for a Drip Irrigated Field by Assimilating Cosmic-ray Neutron Intensity

Xujun Han[1,2], Harrie-Jan Hendricks Franssen[1,2], Miguel Ángel Jiménez Bello[3], Rafael Rosolem[4], Heye Bogena[1], Fernando Martínez Alzamora[3], André Chanzy[5], Harry Vereecken [1,2]

1. Forschungszentrum Jülich, Agrosphere (IBG 3), Leo-Brandt-Strasse, 52425 Jülich, Germany
2. Centre for High-Performance Scientific Computing in Terrestrial Systems: HPSC TerrSys, Geoverbund ABC/J, Leo-Brandt-Strasse, 52425 Jülich, Germany
3. Institute of Water and Environmental Engineering (IIAMA). Universitat Politècnica de Valencia. Camino de Vera, s/n, 46022 Valencia, Spain
4. Department of Civil Engineering, University of Bristol, Bristol BS8 1TR, UK
5. INRA, UMR1114, Environnement Méditerranéen et Modélisation des AgroHydrosystèmes, Domaine Saint Paul, Site Agroparc, F-84914 Avignon, France

Corresponding author: Xujun Han, Forschungszentrum Jülich, Agrosphere (IBG 3), Leo-Brandt-Strasse, 52425 Jülich, Germany. (x.han@fz-juelich.de)

Abstract

Neutron intensity measured by the aboveground cosmic-ray neutron intensity probe (CRP) allows estimating soil moisture content at the field scale. In this work, synthetic neutron intensities were used to remove the bias of simulated soil moisture content or update soil hydraulic properties (together with soil moisture) in the Community Land Model (CLM) using the Local Ensemble Transform Kalman Filter. The cosmic-ray forward model COSMIC was used as the non-linear measurement operator which maps between neutron intensity and soil moisture. The novel aspect of this work is that synthetically measured neutron intensity was used for real time updating of soil states and soil properties (or soil moisture bias) and posterior use for the real time scheduling of irrigation (data assimilation based real-time control approach). Uncertainty of model forcing and soil properties (sand fraction, clay fraction and organic matter density) were considered in the ensemble predictions of the soil moisture profiles. Horizontal and vertical weighting of soil moisture was introduced in the data assimilation in order to handle the scale mismatch between the cosmic-ray footprint and the CLM grid cell.

The approach was illustrated in a synthetic study with the real-time irrigation scheduling of fields of citrus trees. After adjusting soil moisture content by assimilating neutron intensity, the irrigation requirements were calculated based on the water deficit method. Model bias was introduced by using coarser soil texture in the data assimilation experiments than in reality. A series of experiments was done with different combinations of state, parameter and bias estimation in combination with irrigation scheduling.

Assimilation of CRP neutron intensity improved soil moisture characterization. Irrigation requirement was overestimated if biased soil properties were used. The soil moisture bias was reduced by 35% after data assimilation. The scenario of joint state-parameter estimation resulted in the best soil moisture characterization (50% decrease in root mean square error compared to open loop simulations), and the best estimate of needed irrigation amount (86% decrease in Hausdorff distance compared

to open loop). The coarse scale synthetic CRP observation was proven to be useful for the fine scale soil moisture and soil properties estimation for the objective of irrigation scheduling.

Keywords: Data Assimilation; Cosmic ray; Soil Moisture; Parameter Estimation; Bias Estimation; Irrigation Scheduling

1. Introduction

Globally, 70% of fresh water is used by agriculture (FAO - Food and Agriculture Organization of the United Nations). Therefore, it is necessary to increase the water use efficiency and reduce the water need for crop production, while maintaining crop yield. Enough water should be applied to meet the requirement of maximum crop evapotranspiration (ET). Farmers usually base irrigation scheduling on their own experience taking into account soil water status and crop growth. However, it is unlikely that the optimal scheduling of irrigation is acquired without the knowledge of crop water needs. Low cost sensors that measure soil moisture content can be of advantage. However, these sensors typically have a very small measurement volume which is much smaller than the scale of the fields where the crops are grown. Numerical models like crop growth models (Heng et al., 2009) and land surface models (Wood et al., 2011) can be used for the quantitative estimation of the irrigation requirement under specific soil water and crop growth conditions. The estimated irrigation amount can be applied accurately with new agricultural technology like drip irrigation (Sampathkumar et al., 2012). However, uncertain model input data and deficits in the model structure result in biased estimates of soil water status, crop transpiration and therefore irrigation requirement.

The optimal scheduling of irrigation is complicated given the high heterogeneity of soil moisture content in drip irrigated fields. An estimate of soil moisture content for the complete root zone is important in this context. It is difficult to achieve this with small-scale measurements (e.g., TDR-Time Domain Reflectometry,

77 FDR-Frequency Domain Reflectometry or TDT-Time Domain Transmission) as a
78 prohibitively large number of sensors is needed to cover large irrigated areas. Soil
79 moisture information from remote sensing on the other hand is limited to the upper
80 few soil centimeters, and often has a very coarse horizontal resolution (>10 km)
81 (Entekhabi et al., 2010; Kerr et al., 2010; Montzka et al., 2013). A further limitation
82 of satellite-derived soil moisture content is that it is not reliable for highly vegetated
83 areas (Njoku and Chan, 2006) and high uncertainties (Merlin et al., 2009; Montzka et
84 al., 2013). The spatial variability of soil moisture is controlled by soil hydraulic
85 properties, meteorological forcing, land cover patterns and topographic features at
86 different measurement scales. Small scale variability is more driven by soil hydraulic
87 properties while large scale variability is also more driven by the other factors. Hence,
88 strengths and weaknesses of each measurement method rely on the additional
89 uncertainty given by these additional controlling factors (Crow et al., 2012).

90 A new promising method which can determine integral root zone soil moisture
91 from the measured above ground fast neutron intensity (defined as the number of
92 counted neutrons per unit of time – e.g., counts per hour) has been proposed (Zreda et
93 al., 2012). This synthetic study focuses on the assimilation of cosmic-ray probe (CRP)
94 neutron intensity (Bogena et al., 2013; Desilets et al., 2010; Rosolem et al., 2014;
95 Shuttleworth et al., 2013; Zreda et al., 2008; Zreda et al., 2012). Soil moisture
96 measurements at the intermediate scale of the cosmic ray probe have the advantage
97 that they are less affected by small scale variability of soil hydraulic properties. A
98 further advantage is that soil moisture can be determined for a deeper layer (10-70 cm)

99 in higher temporal frequency than remote sensing (Rosolem et al., 2014).

100 Primary cosmic rays originate from our galaxy and eventually collide with
101 atmospheric nuclei, generating secondary cosmic rays mainly consisting of neutrons
102 (Lal and Peters, 1967). Primary cosmic rays create cascades of secondary high-energy
103 neutrons through colliding with atmospheric nuclei and the high-energy neutrons can
104 penetrate the atmosphere and collide with nuclei in soils. These collisions in the soil
105 generate fast neutrons. Some of these fast neutrons are eventually scattered back to
106 the atmosphere and the fast neutron intensity can be measured with the CRP. The
107 measured intensity of fast neutrons above the ground depends strongly on soil
108 moisture content (Hendrick and Edge, 1966; Zreda et al., 2012). CRPs make use of
109 this principle to estimate soil moisture content for an area of about 600 m diameter
110 and variable measurement depth (~10-70 cm) depending on the soil moisture
111 conditions (Zreda et al., 2012).

112 Measured neutron intensities above ground need to be corrected for variations in
113 incoming high-energetic neutrons and atmospheric pressure (Zreda et al., 2012).
114 Moreover, as the measured neutron intensity depends on additional sources of
115 hydrogen (besides of soil moisture), these need to be taken into account in order to
116 isolate the soil moisture signal. Corrections have been proposed for other hydrogen
117 sources like atmospheric vapor (Rosolem et al., 2013), lattice water and organic
118 carbon in the soil (Franz et al., 2013), hydrogen atoms stored in the litter layer
119 (Bogena et al., 2013) and above-ground biomass (Baatz et al., 2015). Data
120 assimilation studies have shown the advantage of using measured multi-source soil

121 moisture observations for improving the soil moisture profile characterization of a
122 land surface model (Crow et al., 2008; De Lannoy et al., 2007b; Han et al., 2012;
123 Huang et al., 2008; Reichle et al., 2008; Walker et al., 2001). Measured neutron
124 intensities have already been used for assimilation in a land surface model to improve
125 estimates of soil moisture profiles, but the model parameters were calibrated a priori
126 (Han et al., 2015a; Rosolem et al., 2014; Shuttleworth et al., 2013).

127 In this paper we will investigate the benefits of assimilating coarse scale (600 m)
128 neutron intensity data into the Community Land Model (CLM) for the application of
129 drip irrigation for citrus trees on a finer scale (100 m) than the CRP scale. The neutron
130 intensity measured by a synthetic CRP affects a larger area than a typical irrigation
131 management unit (1 ha in this work). In order to study the impact of soil moisture data
132 assimilation on irrigation scheduling, the drip irrigation was therefore simulated at a
133 finer spatial scale than the footprint of a CRP. The drip irrigation was applied at the
134 vegetated area and resulted in a very heterogeneous soil moisture distribution with the
135 alternation of patches of wet and dry soil. It is very CPU-intensive to explicitly model
136 the irrigated patches and the non-irrigated parts, and a simplified implementation was
137 adopted in this work, which will be further detailed in the methodology section. In the
138 simulation experiments, CLM was driven by biased soil properties to mimic the
139 intrinsic model uncertainties. The coarse scale CRP neutron intensity observations
140 were used to update the field scale heterogeneous soil moisture field through data
141 assimilation. The joint soil moisture and soil properties (or soil moisture bias)
142 estimation scheme was evaluated. This is important because soil moisture content and

crop transpiration are sensitive to model parameters (Hou et al., 2012; Rosolem et al., 2012; Schwinger et al., 2010). Typically, field measurements of parameter values are scarce and very uncertain, especially because of the scale mismatch between a local measurement and the model scale (Waller et al., 2014). Model parameter estimation in the context of a data assimilation framework was proven to be successful, using either an augmented state vector approach (Chen and Zhang, 2006), dual state parameter estimation (Moradkhani et al., 2005b) or parameter estimation in a loop external to the data assimilation filter (Vrugt et al., 2005). Successful applications are reported for such diverse areas as groundwater hydrology (Franssen and Kinzelbach, 2008; Kurtz et al., 2014; Schöniger et al., 2012), rainfall-runoff models (Moradkhani et al., 2005a; Vrugt et al., 2006), land surface models (Han et al., 2014a; Pauwels et al., 2009), vadose zone hydrology (Montzka et al., 2011; Wu and Margulis, 2013) and atmospheric models (Ruiz et al., 2013). A data assimilation framework can consider uncertain model forcing, model structure and initial conditions, as well as parameter uncertainties. Data assimilation has become a commonly used method for parameter estimation, especially for large scale applications (Wanders et al., 2014).

Joint soil moisture and soil moisture bias estimation has been proven to be helpful for improving data assimilation results (De Lannoy et al., 2007a; Kumar et al., 2012b) like soil temperature assimilation with bias correction (Bosilovich et al., 2007; Reichle et al., 2010). In this study, we also evaluated the impact of the soil moisture bias estimation method (Dee, 2005) on improving the soil moisture assimilation and irrigation scheduling and compared it with joint state-parameter estimation.

In Han et al., 2015a, we studied the joint updating of soil moisture, soil temperature and leaf area index by assimilating CRP neutron intensity and land surface temperature. In this study however, we considered in addition the joint updating of soil moisture and soil properties, or soil moisture and soil moisture bias, and the vertical and horizontal weighting for updating soil moisture in the footprint of a CRP. This implies that in this work states and parameters for many model grid cells in the CRP footprint are updated with a single CRP neutron intensity observation. This is therefore a small multiscale data assimilation experiment with the irrigation scheduling as one of the objectives.

It is expected that a more accurate characterization of the heterogeneous soil moisture distribution can be obtained if the coarse scale CRP neutron intensity data are assimilated using a combination of data assimilation and parameter estimation (or bias estimation). Based on such results, it is then assumed that the estimated irrigation requirement could be improved. The objective of this study is to evaluate with help of a synthetic study: 1) the potential of measured neutron intensity data by the CRP for improving the characterization of soil moisture content and soil properties (or soil moisture bias), and 2) the impact of the assimilation of neutron intensity on better irrigation scheduling and the potential for real-time irrigation optimization. In this study, the spatial variability of soil properties and crop status will be considered in the data assimilation.

2. Methodology

187 The main components of the methodology are: (i) measurement of above-ground
188 neutron intensity, which is linked to field scale soil moisture content by a
189 measurement operator (section 2.1) and horizontal weights (section 2.3); (ii) the land
190 surface model CLM (version 4.5) which simulates the transport of water and energy
191 in the soil-plant-atmosphere continuum (section 2.2); (iii) data assimilation according
192 to the Local Ensemble Transform Kalman Filter (LETKF) methodology (Hunt et al.,
193 2007) which optimally combines measurements and model predictions to update soil
194 moisture (and possibly soil properties or soil moisture bias), taking into account
195 uncertain atmospheric forcing and model parameters (or model bias) (section 2.3) and
196 (iv) an optimization routine which calculates irrigation need for the ensemble of soil
197 moisture forecasts (section 2.4).

198 **2.1. Cosmic ray Soil Moisture Interaction Code (COSMIC)**

199 In order to assimilate neutron intensity, the relationship between neutron intensity
200 and depth-weighted soil moisture content should be reasonably represented. The
201 newly-developed COsmic ray Soil Moisture Interaction Code (COSMIC)
202 (Shuttleworth et al., 2013) was adopted as the forward observation operator to
203 simulate the equivalent neutron count rates from simulated soil moisture profiles (i.e.,
204 soil moisture contents for 10 vertical model layers of CLM from surface to 3 m depth,
205 in this study) and takes into account the weighted contribution of individual soil
206 layers with depth. The COSMIC operator calculates the number of fast neutrons
207 reaching the CRP N_{COSMOS} at a near-surface measurement point by:

$$N_{COSMOS} = N\int_0^{\infty}\left\{A(z)[\alpha\rho_s(z)+\rho_w(z)]\exp\left(-\left[\frac{m_s(z)}{L_1}+\frac{m_w(z)}{L_2}\right]\right)\right\}dz \quad (1)$$

$$A(z) = \left(\frac{2}{\pi}\right)\int_0^{\pi/2}\exp\left(\frac{-1}{\cos(\varphi)}\left[\frac{m_s(z)}{L_3}+\frac{m_w(z)}{L_4}\right]\right)d\varphi \quad (2)$$

$$\alpha = 0.405 - 0.102\times\rho_s \quad (3)$$

$$L_3 = -31.76 + 99.38\times\rho_s \quad (4)$$

where N (counts/h) is the number of high-energy neutrons at the soil surface, z is the soil layer depth (m), ρ_s is the dry soil bulk density (g cm^{-3}), ρ_w is the total soil water density, including the lattice water (g cm^{-3}); $m_s(z)$ and $m_w(z)$ are the integrated mass per unit area of dry soil and water (g cm^{-2}), φ is the angle between the vertical below the detector and the line between the detector and each point in the plane (Shuttleworth et al., 2013), L_1 is the high energy soil attenuation length with value of 162.0 gcm^{-2}, L_2 is the high energy water attenuation length of 129.1 gcm^{-2}, L_3 is the fast neutron soil attenuation length (gcm^{-2}) and L_4 is the fast neutron water attenuation length with value of 3.16 gcm^{-2} (Shuttleworth et al., 2013).

In this study soil moisture contents for 10 vertical soil layers of CLM were used to drive the COSMIC operator. COSMIC interpolates the soil moisture to 300 layers with a soil profile depth of 3 meters and derives the fast neutron count rate from the depth-averaged soil moisture content based on the effective sensor depth, also calculated by COSMIC. The simulated fast neutron intensity was assumed to be observed and subsequently used for the data assimilation as will be explained below. Vertical variation of soil moisture content will be considered according to the contribution to the total neutron intensity of each soil layer.

2.2. Community Land Model - CLM

The Community Land Model (CLM - version 4.5) developed by the National Center for Atmospheric Research (NCAR) was used to calculate soil moisture content and evapotranspiration (Oleson et al., 2013). CLM uses the simplified Richards equation to model water flow in the unsaturated zone and calculation of land surface energy fluxes is done by invoking the Monin-Obukhov similarity theory. In addition, the following processes can be simulated by CLM: transfer of solar radiation and longwave radiation, stomatal physiology and photosynthesis, crop dynamics and irrigation (Oleson et al., 2013). The land cover can be represented by 17 plant functional types (PFTs) and the calculation of energy fluxes is based on the PFTs. Hydraulic and thermal parameters in CLM are derived based on soil properties such as sand and clay fraction and organic matter density (Oleson et al., 2013).

2.3. Data Assimilation and Parameter Estimation

The Local Ensemble Transform Kalman Filter (LETKF) is a square root ensemble Kalman filter (Hunt et al., 2007; Miyoshi and Yamane, 2007), which is applied extensively in atmospheric data assimilation studies (Aravéquia et al., 2011; Baek et al., 2006; Lien et al., 2013; Miyoshi et al., 2014) and also in land data assimilation studies (Han et al., 2014a). In LETKF, the uncertainty of the model forecast is represented by ensemble members. In this study LETKF is used to estimate both soil moisture and soil properties with the state augmentation method (Bateni and

Entekhabi, 2012; Han et al., 2014a; Li and Ren, 2011) or to update soil moisture and soil moisture bias jointly.

First two matrices $\mathbf{X}^b$ and $\mathbf{Y}^b$ are constructed based on simulated soil moisture and soil properties (or soil moisture bias) of the ensemble members:

$$\mathbf{X}^b = \left[\mathbf{x}_1^b - \bar{\mathbf{x}}^b, \ldots, \mathbf{x}_M^b - \bar{\mathbf{x}}^b\right] \quad (5)$$

$$\mathbf{y}_i^b = H\left(\mathbf{x}_i^b\right) \quad (6)$$

$$\mathbf{Y}^b = \left[\mathbf{y}_1^b - \bar{\mathbf{y}}^b, \ldots, \mathbf{y}_M^b - \bar{\mathbf{y}}^b\right] \quad (7)$$

where $\mathbf{x}_1^b, \ldots \mathbf{x}_M^b$ are vectors with the ensemble members, M is the ensemble size, $\bar{\mathbf{x}}^b$ is the vector with ensemble means calculated over $\mathbf{x}_1^b, \ldots \mathbf{x}_M^b$, H is the observation operator (i.e., COSMIC for soil moisture), $\mathbf{y}_i^b$ is the mapping of the ensemble members $\mathbf{x}_1^b, \ldots \mathbf{x}_M^b$ to the measurement space and $\bar{\mathbf{y}}^b$ is the vector of ensemble means of $\mathbf{y}_1^b, \ldots \mathbf{y}_M^b$. The vector $\bar{\mathbf{x}}^b$ contains i) the depth weighted average soil moisture θ_{cosmic}, which was derived from COSMIC and considers the contribution of different soil layers, ii) the soil moisture of 10 layers ($\theta_1 \ldots \theta_{10}$) and iii) soil properties (sand fraction, clay fraction and organic matter density) in case soil properties are estimated. In case of bias estimation, the vector $\bar{\mathbf{x}}^b$ contains soil moisture bias instead of soil properties. The dimensions of the augmented state vector $\bar{\mathbf{x}}^b$ were 11 for the state estimation only, 14 for joint state and parameter estimation, and 12 for joint state and bias estimation. Only soil properties and soil moisture bias for the upper soil layer were included in the state vector $\bar{\mathbf{x}}^b$. Soil properties for all 10 layers were updated based on the ratio of the soil properties between the upper soil layer and the lower soil layers (Han et al., 2014b). The soil moisture bias of deeper

layers was assumed to decrease exponentially according to equation (8).

$$\bar{\mathbf{x}}^{b} = \left\{ \begin{array}{ll} \begin{bmatrix} \theta_{cosmic} \\ \theta_{1} \\ \\ \theta_{10} \end{bmatrix} & state\,estimation \\ \\ \begin{bmatrix} \theta_{cosmic} \\ \theta_{1} \\ \\ \theta_{10} \\ Sand \\ Clay \\ Organic \end{bmatrix} & parameter\,estimation \\ \\ \begin{bmatrix} \theta_{cosmic} \\ \theta_{1} + \theta_{Bias}^{k-1} * exp\left(-1.0 * Z_{1}\right) \\ \\ \theta_{10} + \theta_{Bias}^{k-1} * exp\left(-1.0 * Z_{10}\right) \\ \theta_{Bias}^{k-1} \end{bmatrix} & bias\,estimation \end{array} \right\} \tag{8}$$

where Z_i (m) is the i^{th} soil layer thickness of CLM and k is the time step.

Next, the analysis error covariance matrix $\mathbf{P}^{a}$ is calculated:

$$\mathbf{P}^{a} = \left[\left(M-1\right)\mathbf{I} + \mathbf{Y}^{bT}\mathbf{R}^{-1}\mathbf{Y}^{b}\right] \tag{9}$$

where $\mathbf{R}$ is the observation error covariance matrix. The perturbations in the ensemble space $\mathbf{W}^{a}$ are calculated according to:

$$\mathbf{W}^{a} = \left[\left(M-1\right)\mathbf{P}^{a}\right]^{1/2} \tag{10}$$

The analysis mean $\bar{\mathbf{w}}^{a}$ is given by:

$$\bar{w}^{a} = \mathbf{P}^{a}\mathbf{Y}^{bT}\mathbf{R}^{-1}\left(\mathbf{y}^{o} - \bar{\mathbf{y}}^{b}\right) \tag{11}$$

where $\mathbf{y}^{o}$ is the vector with the measured CRP neutron intensity. The analysis mean is added to each column of $\mathbf{W}^{a}$ to get the analysis ensemble.

Finally, the new analysis $\mathbf{X}^{a}$ is obtained according to:

$$\mathbf{X}^a = \mathbf{X}^b \mathbf{W}^a + \bar{\mathbf{x}}^b \quad (12)$$

where $\mathbf{X}^a$ are the model ensemble members after analysis. $\mathbf{X}^a$ includes the updated soil moisture and soil properties (or soil moisture bias), and will be used as initial condition for the next time step.

The forecast model of soil moisture bias $\boldsymbol{\theta}_{Bias}^k$ was defined as:

$$\boldsymbol{\theta}_{Bias}^k = \boldsymbol{\theta}_{Bias}^{k-1} \quad (13)$$

where k is the time step.

In this study, the LETKF was applied as a 1D filter to update soil moisture in the cosmic ray footprint, which covered several fine scale model grid cells. Neutron intensity data were used to update the fine scale soil moisture within the expected CRP footprint and the contribution of different grid cells within the CRP footprint to the observed neutron intensity was taken into account by assigning different horizontal weights to the CLM grid cells. Following the horizontal weighting method proposed by (Bogena et al., 2013), we used a Gaussian window function (Harris, 1978) to define the horizontal weights of the different CLM grid cells in the CRP footprint. Because a single observation was used to update the soil moisture content of many CLM grid cells, a simple multi-scale data assimilation strategy was proposed. First, the COSMIC operator was run for each CLM grid cell to simulate the neutron intensity of each CLM grid cell. Next, a convolution with a Gaussian window function was applied to retrieve the integrated neutron intensity at the coarse scale. This convolution step was used in both the ensemble runs and the parallel runs (introduced in section 3.3). Therefore the CRP neutron intensity (measured/simulated)

considered the contributions from all model grid cells contained within the CRP footprint. The size of the Gaussian window function was chosen as the diameter of the CRP footprint (600 m). The observation operator *H* (needed by equation (6)) was defined as the combination of a Gaussian window function and the COSMIC operator. Using equation (6) we get:

$$\mathbf{y}_i^b = f_{Gaussian}(f_{cosmic}\left(\mathbf{x}_i^b\right)) \quad (14)$$

where f_{cosmic} represents the COSMIC operator and $f_{Gaussian}$ the Gaussian window function.

The footprint of the CRP covered 43 CLM grid cells (i.e., ~600 m diameter). The data assimilation was done grid cell by grid cell in LETKF. Therefore the time series of a single neutron intensity observation was assigned uniformly to all grid cells of the CRP footprint and then the observations were assimilated separately for each CLM grid cell. The spatial localization was applied on the model states using equation (14), and therefore the observation localization was not used in this study (Greybush et al., 2011; Han et al., 2015b). The soil moisture measured by CRP is composed of the contribution of all horizontal and vertical CLM grid cells of the CRP footprint. Therefore, there is only one relevant soil moisture content value and neutron intensity value. Given equation (14), the upscaling of soil moisture from CLM will be done before assimilation, it means the upscaled soil moisture θ_{cosmic} which incorporates the contribution from all surrounding grid cells will be used as the soil moisture content value to be updated with the CRP neutron intensity measurement. All the soil moisture content values for the individual grid cells within the CRP footprint (both

horizontally and vertically) will be updated according to the correlation between the simulated values by CLM and θ_{cosmic}:

$$\theta_{cosmic} = f_{Gaussian}(f_{cosmic}(\mathbf{x}_i^b)) \quad (15)$$

2.4. Irrigation Requirement

CLM computes the water deficit between the current soil moisture content and a target soil moisture content. The target soil moisture in each soil layer is a weighted average of (1) the minimum needed soil moisture content to avoid water stress for that layer and (2) the saturated soil moisture content for that layer (Levis and Sacks, 2011):

$$\theta_{target,i} = (1-0.7)\times\theta_{o,i} + 0.7\times\theta_{sat,i} \quad (16)$$

where i is the soil layer number, $\theta_{o,i}$ is the minimum soil moisture content of each vegetation type so that stomata are completely opened and $\theta_{sat,i}$ is the effective soil porosity.

The total water deficit $W_{deficit}$ (mm) was defined as:

$$W_{deficit} = \sum_{i}^{N} Root\_Fraction_i \times \max(\theta_{target,i} - \theta_{liq,i}, 0) \quad (17)$$

where $\theta_{liq,i}$ is the current soil moisture content of layer i.

The estimated irrigation amount $W_{deficit}$ was applied in CLM as an incoming water flux not subjected to interception by the canopy layer (precipitation on the contrary was subjected to interception).

The root fraction (RF_i) of citrus trees for the soil layer i was parameterized as (Oleson et al., 2013):

352 $$RF_i = \begin{cases} 0.5\left[\begin{array}{l}\exp\left(-r_a Z_{h,i-1}\right)+\exp\left(-r_b Z_{h,i-1}\right)\\ -\exp\left(-r_a Z_{h,i}\right)+\exp\left(-r_b Z_{h,i}\right)\end{array}\right] & 1 \le i < N_{levsoi} \\ 0.5\left[\exp\left(-r_a Z_{h,i-1}\right)+\exp\left(-r_b Z_{h,i-1}\right)\right] & i = N_{levsoi} \end{cases} \quad (18)$$

353 where $Z_{h,i}$ (m) is the depth from the soil surface to the interface between soil
354 layers i and $i+1$ ($Z_{h,0}=0$ represents the soil surface), r_a and r_b are plant
355 dependent root distribution parameters, for citrus trees: $r_a = 8.992$, $r_b = 8.992$ (Zeng,
356 2001), $N_{levsoi} = 10$ is the total number of soil layers.

357

358 **2.5. Performance Measures**

359 In order to evaluate the results of data assimilation and irrigation, the Root Mean
360 Square Error (RMSE) was calculated for the hourly soil moisture results:

361 $$\mathrm{RMSE} = \sqrt{\frac{\sum_{k=i}^{K}\left(\theta_{est} - \theta_{ref}\right)^2}{K}} \quad (19)$$

362 where θ_{est} is the hourly soil moisture ensemble mean for a given scenario, θ_{ref}
363 is the hourly soil moisture value of the reference scenario. *K* is equal to 8760. Soil
364 moisture contents at the time points of assimilation and prediction were included in
365 the calculations with Eq. 19. Lower RMSE values mean better performance.

366 The Hausdorff Distance (HD) is a quantitative measure of the similarity between
367 two spatial distributions (Kumar et al., 2012a). Lower HD values mean higher spatial
368 similarity. HD is defined as the maximum distance of a set to the nearest point in the
369 other set:

370 $$h(Q,R) = \max_{q \in Q}\left\{\min_{r \in Q}\{q-r\}\right\} \quad (20)$$

371 where $h(Q,R)$ is the HD value and q and r are the points of sets Q and

372 R. $q-r$ is the norm of the points in the space of Q and R, in terms of Euclidean
373 distance. Q is the estimated annual irrigation amount of a CLM grid cell in the CRP
374 footprint and R is the annual irrigation amount of the reference scenario of the CRP
375 footprint.

376 The t-test can be used to determine whether two data sets are significantly
377 different. The independent two-sample t-test was used to evaluate the statistical
378 significance of the difference between the estimated irrigation amount and the
379 reference irrigation amount (Welch, 1947). The definition of the t-test is as follows:

380 $$t = \frac{\bar{X}_1 - \bar{X}_2}{\sqrt{\frac{s_1^2}{N_1} + \frac{s_2^2}{N_2}}} \quad (21)$$

381 where $\bar{X}_1 / \bar{X}_2$, s_1^2 / s_2^2 and N_1 / N_2 are the mean, variance and the number of
382 optimized irrigation amounts, respectively. The subscripts 1 and 2 represent the
383 reference scenario and estimation scenario, respectively.

384

385 **3. Synthetic Experiment**

386 A synthetic study was conducted to evaluate the methodology outlined in the
387 previous sections. The synthetic study mimicked the Picassent site (close to Valencia,
388 Spain) with citrus trees, which receives drip irrigation. The site is situated in a
389 semi-arid region (39.38^o N, 0.47^o E) with yearly average precipitation of 454 mm (44
390 precipitation days), average daily maximum temperature of 22.3^{o}C and average daily
391 minimum temperature of 13.4^{o}C, and with a yearly irrigation period from April to
392 October. In the synthetic experiments, a CRP (Zreda et al., 2012) measured the

393 neutron intensity which was assimilated in the land surface model CLM.

394

395 **3.1. Design of Synthetic Experiments**

396 The citrus tree was modeled as a broadleaf evergreen tropical PFT in CLM. In
397 order to mimic the planting pattern of citrus trees at the Picassent site, odd CLM grid
398 columns were modelled as bare ground without vegetation cover while even CLM
399 columns were modelled as fully covered by broadleaf evergreen tropical trees. The
400 mimicked ground cover of vegetation was similar to the real measured ground cover
401 fraction of citrus trees. Soil properties (sand fraction and clay fraction) and organic
402 matter density determine the soil thermal and hydraulic properties in CLM. Soil
403 samples from the Picassent region were taken and a soil sand fraction of 32%, clay
404 fraction of 33%, bulk density of 1.5 gcm^{-3}, and organic fraction of 1.2% (10 cm depth)
405 and 0.7% (50 cm depth) were determined using the Bouyoucos method, which is
406 based on stokes law and involves use of a hydrometer (Bouyoucos, 1962) and applied
407 uniformly in space in CLM. Spatially correlated noise was added to the uniform soil
408 properties to represent the spatial heterogeneity. The noise was simulated by
409 sequential Gaussian simulation with a correlation range of 100 m, variance of 100.0
410 (%) and mean value of 0.0 (%). The noise was constrained within the range of (-5.0%,
411 5.0%) after the sequential Gaussian simulation. The atmospheric forcing data
412 measured by the Picassent weather station were used as CLM input. The maximum
413 rate of carboxylation at 25 °C (V_{cmax25}) controls the maximum rate of carboxylation
414 and canopy transpiration in CLM. The default value of V_{cmax25} is 55 $\mu molm^2s^{-1}$ for

broadleaf evergreen tropical tree in CLM. It was changed to 100 $\mu molm^2s^{-1}$ according to a reference value for citrus trees (Velikova et al., 2012). The study area was discretized in 40×60 grid cells at a spatial resolution of 100 m. However, our analysis will focus on the CRP footprint which contains only 43 CLM grid cells in total. Because of the spatial discretization, it is not easy to describe the exact CRP footprint. The diameter of the CRP footprint for the horizontal weighting calculation was chosen as the ratio between the CRP diameter and the spatial resolution of the CLM grid cell, which was 7 grid cells.

A model spin-up was made to obtain reasonable initial conditions for CLM. CLM was run for the spin-up period from 2010-01-01 to 2010-12-31 using an hourly time step. Next, a one-year (2011-01-01 to 2011-12-31) irrigation estimation using the true soil properties was performed in CLM and the irrigation requirement was calculated every three days during the period from 2011-01-01 to 2011-12-31 and subsequently applied. This reference model run also supplied the reference soil moisture distribution in space and time and the canopy transpiration, and a distribution in space and time (and total amounts) of irrigation.

3.2. Ensemble Generation

The simulation experiments evaluated how well the soil moisture, evapotranspiration, soil properties and irrigation requirement could be characterized if soil properties and model forcing were biased and/or uncertain, but the measurement data (albeit synthetically generated for this study) in the form of CRP neutron

intensity were available. We assumed that the soil texture was systematically coarser than in reality. The soil properties used in the reference run were perturbed to represent these conditions: the sand fraction was multiplied by 1.5 while the clay fraction and organic matter density were both multiplied by 0.75. In addition, for all scenarios the sand and clay fractions, and organic matter density were perturbed by a uniform distributed noise in the range of [-10.0%, 10.0%] (for soil texture) and [-10.0 km m^{-3}, 10.0 km m^{-3}] (for organic matter density) to generate 20 different soil hydraulic properties for the 20 different ensemble members. It is assumed that these perturbations represent a realistic representation of the uncertainty in practice. If the sum of the sand and clay fraction was larger than 98%, an amount equal to ((Sand%+Clay%) – 98%)/2.0 was subtracted from both the sand and the clay fraction. For the ensembles for which initial soil moisture bias was updated instead of soil properties, soil moisture was perturbed with a spatially uniform value sampled from the uniform distribution with values between -0.04 m^3m^{-3} and 0.04 m^3m^{-3}.

The atmospheric forcing data of precipitation, air temperature, shortwave incident radiation and longwave incident radiation were perturbed with a noise correlated in space and time (Han et al., 2013). The spatially correlated noise was generated using the Fast Fourier Transform approach and the temporal correlation was imposed by a first-order auto-regressive model approach (Kumar et al., 2009; Park and Xu, 2009). The perturbation parameters are summarized in Table 1.

3.3. Synthetic Observation

In this study, the "observed" synthetic CRP neutron intensity was generated using the COSMIC model, which used the soil moisture profile simulated by CLM as input. A point which had to be considered in the simulation scenarios was that the soil moisture changed also as response to the irrigation amount applied in the CLM simulation. Therefore, the synthetic observations will be different for each simulation scenario due to the different irrigation amounts. In order to obtain the synthetic measurements of CRP neutron intensity for these scenario runs, a parallel run was made with the same soil properties and atmospheric forcing as the reference run for each of the simulation scenarios. However, the irrigation amount for this parallel run was the same as the optimized one for the specific simulation scenario. Therefore irrigation amounts differed among the parallel runs of the different scenarios. This in turn also affected the CRP intensity which was assimilated in the simulation scenarios. The soil moisture calculated in the parallel run was used now as the synthetic soil moisture measurement for this specific scenario and also used as input for COSMIC to estimate the synthetic CRP neutron intensity. This implies that the assimilated CRP neutron intensity differed among different scenarios, in correspondence with different irrigation amounts applied in the different scenarios.

In this synthetic study, N_{COSMOS} was set to 150 counts h^{-1} and lattice water was 3% in COSMIC. The simulated CRP intensity measurements were perturbed in order to represent the observation error. This perturbation had a mean equal to zero and a variance equal to the square root of the neutron intensity to represent the observation error. The CLM grid cells located in the footprint of the CRP were updated by the data

481 assimilation procedure. The neutron intensity observation was assimilated at 23:00
482 each three days, prior to irrigation scheduling.
483 Fig. 1 shows a schematic overview of the complete calculation procedure for each
484 time step.
485 [Insert Figure 1 here]
486
487 **3.4. Irrigation Scheduling**
488 In Valencia, citrus trees are typically irrigated 3~6 days per week from April to
489 October. For simplicity, the irrigation duration was assumed to be two hours from
490 06:00 AM onwards, and the irrigation was applied every three days for reasons of
491 computational efficiency. CLM was run in prediction mode for three days to estimate
492 the needed amount of irrigation (at 06:00) using the predefined atmospheric forcing
493 data. The first assimilation of soil moisture data was done at 23:00, seven hours
494 before the start of the second irrigation period.
495 Five irrigation estimation scenarios were designed to assimilate the CRP neutron
496 intensity in the land surface model and to evaluate the impact of data assimilation,
497 parameter estimation and bias estimation on the characterization of the soil moisture
498 profile, irrigation amount and evapotranspiration:
499 (1) Irrigation estimation with the true soil properties and atmospheric forcing
500 (Reference).
501 (2) Irrigation estimation with biased soil properties, without CRP neutron
502 intensity assimilation (No_DA, i.e. Open loop).

(3) Irrigation estimation with biased soil properties, with the assimilation of CRP neutron intensity (every three days) (Only_DA_SM).

(4) Irrigation estimation with biased soil properties, with both CRP neutron intensity assimilation (every three days) and soil moisture bias estimation (DA_SM_Bias).

(5) Irrigation estimation with biased soil properties, with neutron intensity assimilation (every three days) including soil properties estimation (DA_SM_Par). For the scenario of DA_SM_Par, the study period included both 2010 and 2011. In 2010, joint soil moisture and soil properties estimation were carried out in order to update the biased soil properties (sand fraction, clay fraction and organic matter density). Next, in 2011 the updated soil properties were used for soil moisture assimilation without soil properties updating. For the scenarios without soil properties estimation, the experiments were only carried out for 2011.

The estimation of soil properties during the year 2010 deteriorated in case of intensive irrigation. In case of intensive irrigation, the soil column is close to saturation, and the ensemble members show a limited spread. In addition, the sensitivity of soil moisture with respect to soil properties becomes small. Parameter estimation (i.e., updating of soil properties) is not very efficient during these periods. Therefore, soil properties were not updated if the accumulated irrigation amount between two data assimilation time steps was larger than 10 mm.

4. Results

525 In this section we evaluate time series for the different simulation scenarios at the
526 CRP location. Spatial patterns of (estimated) soil properties and optimized irrigation
527 amounts for different simulation scenarios are also compared. This comparison is
528 made at the scale of the complete CRP footprint. The temporal evolution of soil
529 moisture content at 30 cm and 50 cm depth for different simulation scenarios is shown
530 in Fig. 2. The scenario No_DA underestimated soil moisture content even although
531 (too) high irrigation amounts were scheduled, which is related to the erroneous soil
532 texture in this simulation scenario and the associated bias in soil properties like
533 saturated hydraulic conductivity. In the data assimilation scenario Only_DA_SM soil
534 moisture characterization was improved by assimilating the CRP neutron intensity,
535 but the bias was also very high due to the large bias of soil properties. In order to
536 reduce the soil moisture bias, the joint soil moisture state and bias estimation was
537 evaluated in the scenario DA_SM_Bias by use of the state augmentation method. The
538 soil moisture estimation became better than Only_DA_SM after the soil moisture bias
539 was reduced. The best soil moisture results were obtained in the scenario DA_SM_Par,
540 in which sand fraction, clay fraction and organic matter density were updated
541 sequentially using the joint state and parameter estimation method.

542 [Insert Figure 2 here]

543 The RMSE values for soil moisture characterization are summarized in Fig. 3.
544 Compared with the Reference scenario, the scenarios No_DA and Only_DA_SM
545 underestimated soil moisture content, which resulted in higher irrigation requirement
546 than for the reference case. Compared with the scenario No_DA, the RMSE values

547 for soil moisture content at 30 cm depth decreased by 33%, 40% and 52% for the
548 scenarios Only_DA_SM, DA_SM_Bias and DA_SM_Par, respectively. At 50cm
549 depth these RMSE-decreases were 39%, 35% and 51% for the scenarios
550 Only_DA_SM, DA_SM_Bias and DA_SM_Par, respectively. These results illustrate
551 the benefit of joint state-parameter estimation. Model results were strongly influenced
552 by the biased soil properties for the scenario Only_DA_SM, where measurement data
553 were not used to estimate model bias or soil properties. As model bias was related to
554 biased soil properties in these simulations, joint state and parameter estimation
555 performed better than the scenario with joint state and bias estimation.

556 [Insert Figure 3 here]

557 Fig. 4 shows the soil moisture bias for the different ensemble members (scenario
558 DA_SM_Bias). The temporal evolution of the bias is shown for the first soil layer and
559 the CRP location. The time series of true soil moisture bias (the scenario No_DA) is
560 shown for comparison. The mean bias value for No_DA is 0.051 m^3m^{-3} and 0.033
561 m^3m^{-3} for DA_SM_Bias. The joint state-bias estimation could reduce 35% of the soil
562 moisture bias introduced by the biased soil properties.

563 [Insert Figure 4 here]

564 The CLM model derives the soil hydraulic parameters using a predefined
565 pedotransfer function (Oleson et al., 2013). The updated soil texture resulted therefore
566 in updated soil hydraulic parameters in CLM. In order to show the influence of
567 calibrated soil texture on the soil hydraulic parameters, the temporal evolution of the
568 calibrated saturated hydraulic conductivity K and the empirical parameter B which

represent the slope of water retention curve in the Clapp–Hornberger parameterization (Clapp and Hornberger, 1978; Oleson et al., 2013) are shown in Fig. 5 (scenario DA_SM_Par). The Clapp–Hornberger parameterization can be used to calculate the hydraulic conductivity when the soil water retention data are not available. All soil hydraulic parameters could be improved in this scenario by assimilating the CRP neutron intensity. The mean ensemble values for the soil hydraulic parameters approached the reference values over the assimilation period. As the soil properties were not updated during the intensive irrigation period, the convergence was slow.

[Insert Figure 5 here]

Fig. 6 shows the time series of irrigation amount at the location of the CRP for the reference case and for the different estimation scenarios. The reference irrigation amount (707.2 mm) was calculated in CLM on the basis of the water deficit method. Fig. 6 illustrates that the intensive irrigation period from June to October coincided with limited precipitation. The reference irrigation amount was around twice of the annual precipitation amount (356.1 mm). The sum of the reference irrigation amount (707.2 mm) and annual precipitation (356.1 mm) was about 6% higher than the documented potential annual evapotranspiration of citrus trees (Ballester et al., 2011; Jimenez-Bello et al., 2015). We used a t-test to compare the estimated annual irrigation requirements by the different scenarios with the reference case. Large p values (Fig. 6) indicate that the scenarios with data assimilation did not have a significantly different irrigation scheduling as compared with the reference case. The scenario No_DA has a p value <0.05, which indicates that the estimated irrigation

591 amounts were significantly different from the reference case. Data assimilation
592 (Only_DA_SM) improved results with higher p values (p=0.205). Scenarios with bias
593 correction (p=0.819) and parameter estimation (p=0.755) gave better results than the
594 scenario of state estimation only (Only_DA_SM). The annual irrigation amounts for
595 the grid cell at the location of the CRP are summarized in Fig. 7. Obviously, joint soil
596 moisture and bias (or parameter estimation) improved the characterization of
597 irrigation requirement.

598 [Insert Figure 6 here]

599 [Insert Figure 7 here]

600 Now we analyze the irrigation results for the scenarios in detail. The better
601 characterization of the irrigation demand was found by combining CRP neutron
602 intensity assimilation and soil properties estimation (or soil moisture bias estimation).
603 Scenarios DA_SM_Bias and DA_SM_Par estimated an irrigation requirement of
604 691.0 mm and 685.6 mm, respectively. The scenario Only_DA_SM (i.e., data
605 assimilation with state estimation only) gave an irrigation estimation of 797.7 mm.
606 CRP neutron intensity assimilation without parameter estimation provided much
607 better results than scenarios without data assimilation (No_DA). The estimated
608 irrigation amount for the scenario No_DA was 1107.3 mm. These results illustrate that
609 irrigation estimation for the case of biased soil properties (i.e., sandier soil in model
610 than in reference run) can be improved significantly by the assimilation of CRP
611 neutron intensity and even better by including soil properties estimation or bias
612 estimation. Data assimilation improved the estimation of irrigation demand and even

613 resulted in a slightly lower irrigation than for the reference case.

614 The CRP footprint was composed of 43 CLM grid cells which were irrigated
615 separately. The irrigation requirements estimated for the different scenarios are
616 displayed in Fig. 8 and compared with the reference scenario. The spatial irrigation
617 patterns of scenarios DA_SM_Bias and DA_SM_Par are closer to the reference case
618 than the scenario without data assimilation (No_DA).

619 [Insert Figure 8 here]

620 The single CRP neutron intensity measurement for the coarse scale (600 m) was
621 used to update the 43 CLM grid cells at the fine scale (100 m). The spatial distribution
622 of soil properties and annual irrigation amount were compared with the reference
623 spatial distributions. A higher spatial similarity is associated with lower HD values.
624 The HD values were evaluated according to the distance between a CLM grid cell and
625 the CRP location. Three classes were defined: (i) distance CRP- grid cell $\leq$ 100 m; (ii)
626 distance CRP- grid cell > 100 m and $\leq$ 200 m; (iii) distance CRP- grid cell > 200 m
627 and $\leq$ 300 m. The HD values for the comparison of the spatial patterns of soil
628 properties for the scenarios No_DA and DA_SM_Par are shown in Fig. 9. The
629 similarity of soil properties between background and reference is small due to the
630 imposed bias, and the HD values were 580.83, 1186.53, 1203.93 for sand fraction,
631 clay fraction and organic matter density, respectively. The scenario DA_SM_Par
632 resulted in a spatial distribution of soil properties closer to the reference case, with
633 HD values of 69.83 for sand fraction (580.83 for No_DA), 149.96 for clay fraction
634 (1186.53 for No_DA) and 185.21 for organic matter density (1203.93 for No_DA)

635 HD values for sand fraction, clay fraction and organic matter density for the region
636 with distance CRP- grid cell ≤ 100 m decreased by 80%, 82% and 64%, compared to
637 No_DA, respectively. For the region with distance CRP- grid cell > 100 m and ≤ 200
638 m the decreases were 82%, 66% and 67%, respectively. Finally, for the region with a
639 distance CRP- grid cell > 200 m and ≤ 300 m the decreases were 78%, 82% and 40%,
640 respectively.

641 Figure 10 shows the HD values for the comparison of the spatial distribution of
642 irrigation amounts with the reference. The figure includes comparisons for all
643 different data assimilation scenarios. It is clear that the assimilation of CRP neutron
644 intensity (Only_DA_SM) increased the similarity between the spatial distribution of
645 estimated annual irrigation amount and the reference irrigation distribution. Soil
646 properties estimation and soil moisture bias estimation increased the similarity in
647 spatial irrigation pattern further. The HD values for the scenario DA_SM_Bias
648 decreased 89% (distance CRP- grid cell ≤ 100 m), 81% (distance CRP- grid cell > 100
649 m and ≤ 200 m) and 82% (distance CRP- grid cell > 200 m and ≤ 300 m) compared to
650 No_DA. The HD values for the scenario DA_SM_Par, for the same three distance
651 classes and in the same order, decreased by 88%, 87% and 85% compared to No_DA.

652 [Insert Figure 9 here]

653 [Insert Figure 10 here]

654 The total annual ET for the different scenarios was also calculated, and also the
655 contributions from ground evaporation, evaporation of intercepted water by the
656 canopy and canopy transpiration. The ET for the reference scenario was 756.6 mm.

The ET for all other scenarios was very close to the reference. In case of the scenario No_DA, too much water was irrigated so that drought stress did not occur. The other scenarios with data assimilation resulted in less irrigation, but ET was also close to the reference value, indicating that less irrigation was not associated with plant stress. For all the scenarios, the ET values did not deviate much from the reference value. This is because in all cases an overestimation of the percentage of sand led to excessive irrigation and sustainment of potential ET. The largest contribution to the ET was the canopy transpiration. The irrigated grid cells were assumed to be fully covered by the vegetation, and therefore the ground evaporation was low. The low evaporation from the canopy intercepted water maybe related to the fact that the rain events occurred mainly in the spring and winter seasons.

5. Discussion

The proposed data assimilation and parameter estimation (or bias estimation) can improve the soil moisture and irrigation estimation. The joint state-parameter estimation is the best scenario, and reduced the RMSE values of soil moisture content more than 50%, the spatial similarity of irrigation amount was increased and the HD values were decreased by 86% on average. The novelty of this work was the assimilation of the new CRP data in combination with irrigation scheduling. In general, classical parameter estimation tends to focus on uncertainty in the parameter estimates only, while neglecting partial or all of the other uncertainty sources (Liu and Gupta, 2007). We did not aim to compare the parameter estimation methodology with

679 other methodologies in this study. The synthetic CRP neutron intensity observations
680 were assimilated in CLM and the synthetic study potentially overestimated the
681 performance of the proposed method.

682 In a real-world application, the model will show systematical biases and also the
683 implementation of the project area in the model is a strong simplification which might
684 generate additional bias. A complication for the application of the data assimilation
685 system in a real-world application is therefore the presence of model structural bias,
686 and parameter estimation could compensate for this bias so that the estimated
687 parameter values are not necessarily closer to the true parameter values. The approach
688 will try to identify the effective parameter values that maximize model performance at
689 that scale (Wagener et al., 2007). Therefore, as an alternative, instead of updating
690 states and parameters jointly, also states and bias could be estimated jointly. It was
691 shown in this paper that both approaches gave improvements. Although uncertainty of
692 soil hydraulic parameters is important in the context of irrigation scheduling, it might
693 be difficult to infer better estimates of soil hydraulic parameters due to other sources
694 of uncertainty like model structural bias. On the other hand, this does not need to
695 hamper successful operational implementation of the proposed method. Hendricks
696 Franssen et al (2011) demonstrated the feasibility of operational prediction of
697 groundwater levels (Franssen et al., 2011), coupled to operational optimization of
698 groundwater management at the same site (Bauser et al., 2012). The water works
699 Zurich applied this methodology (Franssen et al., 2011) now for the period 2009-2015,
700 with consistent better predictions than for the open loop run. However, in the

operational implementation on-line parameter estimation was avoided and only states were updated. It is therefore possible that for on-line irrigation scheduling a conservative, potentially less successful strategy should be followed where only states are updated. This synthetic study showed that state updating only also would improve irrigation scheduling considerably. We believe therefore that although in a real-world case study results will be less favorable than in the synthetic study, data assimilation with updating states only, or joint updating of states and bias (or parameters) in case of a systematic bias, will improve irrigation scheduling compared to a scenario without data assimilation.

An additional challenge for the real world application is the forward modeling of the CRP neutron intensity. The measured CRP neutron intensity needs to be corrected for variations in the incoming high-energetic neutrons, the atmospheric pressure and humidity, lattice water and organic carbon content of the soil, and aboveground biomass. The aboveground biomass of citrus trees is temporally variable related to the growth of the oranges (or lemons) over the year. The impact of vegetation water content on the CRP neutron intensity is still under active study. In principle, an empirical methodology is suited to correct for the influence of aboveground biomass on measured neutron count intensity (Baatz et al., 2015). In this study, the synthetically measured CRP neutron intensity was applied uniformly at the CRP footprint and a simple multiscale data assimilation scheme was proposed to update the field scale CLM simulation using coarse scale CRP neutron intensity. This may not be optimal as all the grid cells within the CRP footprint contribute differently to the

measured CRP neutron intensity. The soil spatial heterogeneity in the CRP footprint was introduced by adding a random spatially correlated noise. Heterogeneous land cover was not considered in this study. However, the spatial variability of ecosystem parameters could be a further confounding parameter influencing the results. Altogether, accounting for temporally variable biomass in the COSMIC operator does not seem a large limitation, but spatially variable soil moisture conditions within the cosmic ray probe footprint, are a serious challenge.

Furthermore, the weather forecast is essential to the irrigation scheduling. This aspect was not considered in this work. If the precise precipitation forecast cannot be obtained, the irrigation requirement cannot be estimated accurately.

A further important complication for real-world applications is that farmers want to irrigate the citrus based on their own experience, and in combination with the low water prices they might not want to follow the suggested irrigation scheduling. Altogether, we feel that the methodology is suited for real-world applications and can improve irrigation scheduling compared to more traditional scheduling, but that the farmer participation is the most critical factor, besides model structural bias and soil moisture heterogeneity within the cosmic ray probe footprint.

Therefore, the successful real application of the proposed method needs: a calibrated land surface model, an improved COSMIC operator in which the measured cosmic-ray neutron intensity is corrected for above and below ground biomass, not too large spatial variability of soil moisture content within the cosmic ray probe footprint and a precise weather forecast including uncertainty characterization and

745 participation of farmers.

746 A further possible improvement is the consideration of irrigation below ET
747 requirement, known as deficit irrigation (DI), which can reduce water demand to meet
748 the maximum ET (Fereres and Soriano, 2007).

749

750 **6. Conclusions**

751 This study investigated the assimilation of synthetic measurements of coarse
752 scale CRP neutron intensity in CLM for updating field scale root zone soil moisture
753 content. The synthetic study mimicked a drip irrigated citrus farmland near Valencia,
754 Spain. CLM was driven by biased soil properties and the joint estimation of soil
755 moisture and soil properties (or soil moisture bias) was evaluated in a data
756 assimilation framework using the state augmentation method. The non-linear
757 measurement operator COSMIC was used to simulate the CRP neutron intensity on
758 the basis of the soil moisture profile estimated by the CLM model. Fast neutron
759 intensity was assimilated directly, and both soil moisture and soil properties (soil
760 moisture bias) were updated using the LETKF in combination with the CLM model.
761 The horizontal and vertical weights for the different CLM grid cells in the CRP
762 footprint were also considered using a Gaussian window function.

763 The results show that assimilating CRP neutron intensity can improve joint soil
764 moisture and soil properties estimation, and irrigation scheduling. Data assimilation
765 schemes that remove soil moisture bias or update soil properties on the basis of CRP
766 neutron intensity outperform data assimilation without bias or parameter estimation.

The joint soil moisture and soil parameter estimation with simple multiscale assimilation strategy of CRP neutron intensity can potentially be used for irrigation scheduling in the future. The main challenges for the real world application are: model calibration to remove the bias, forward modeling of cosmic-ray neutron intensity under high vegetation coverage, precise weather forecasts and cooperation of farmers.

Acknowledgments

This work was supported by AGADAPT (adapting water use by the agriculture sector) financed by Climate Knowledge and Innovation Community (Climate-KIC) of the European Union. AGADAPT focuses on the development and deployment of novel methods to reduce and optimize the water usage of rain-fed and irrigated agriculture by combining knowledge-based innovative technologies, modelling and transfer of technologies and innovative practices. The work was also supported by Transregional Collaborative Research Centre 32, and the NSFC project (grant number: 41271357, 91125001). The support of the supercomputing facilities of Forschungszentrum Julich (JUROPA) is gratefully acknowledged.

References:

Aravéquia, J.A. et al., 2011. Evaluation of a Strategy for the Assimilation of Satellite Radiance Observations with the Local Ensemble Transform Kalman Filter. Mon Weather Rev, 139(6): 1932-1951.

Baatz, R. et al., 2015. An empirical vegetation correction for soil water content quantification using cosmic ray probes. Water Resour Res, 51(4): 2030-2046.

Baek, S.J., Hunt, B.R., Kalnay, E., Ott, E., Szunyogh, I., 2006. Local ensemble Kalman filtering in the presence of model bias. Tellus A, 58(3): 293-306.

Ballester, C., Castel, J., Intrigliolo, D.S., Castel, J.R., 2011. Response of Clementina de Nules citrus trees to summer deficit irrigation. Yield components and fruit composition. Agr Water Manage, 98(6): 1027-1032.

Bateni, S.M., Entekhabi, D., 2012. Surface heat flux estimation with the ensemble Kalman smoother: Joint estimation of state and parameters. Water Resour Res, 48.

Bauser, G. et al., 2012. A comparison study of two different control criteria for the real-time management of urban groundwater works. J Environ Manage, 105: 21-9.

Bogena, H.R., Huisman, J.A., Baatz, R., Hendricks Franssen, H.J., Vereecken, H., 2013. Accuracy of the cosmic-ray soil water content probe in humid forest ecosystems: The worst case scenario. Water Resour Res, 49(9): 5778-5791.

Bosilovich, M.G., Radakovich, J.D., da Silva, A., Todling, R., Verter, F., 2007. Skin temperature analysis and bias correction in a coupled land-atmosphere data assimilation system. J Meteorol Soc Jpn, 85A: 205-228.

Bouyoucos, G.J., 1962. Hydrometer Method Improved for Making Particle Size Analyses of Soils1. Agron J, 54(5): 464.

Chen, Y., Zhang, D.X., 2006. Data assimilation for transient flow in geologic formations via ensemble Kalman filter. Adv Water Resour, 29(8): 1107-1122.

Clapp, R.B., Hornberger, G.M., 1978. Empirical equations for some soil hydraulic properties. Water Resour Res, 14(4): 601-604.

Crow, W.T. et al., 2012. Upscaling Sparse Ground-Based Soil Moisture Observations for the Validation of Coarse-Resolution Satellite Soil Moisture Products. Rev Geophys, 50(2): n/a-n/a.

Crow, W.T., Kustas, W.P., Prueger, J.H., 2008. Monitoring root-zone soil moisture through the assimilation of a thermal remote sensing-based soil moisture proxy into a water balance model. Remote Sens Environ, 112(4): 1268-1281.

De Lannoy, G.J.M., Houser, P.R., Pauwels, V.R.N., Verhoest, N.E.C., 2007a. State and bias estimation for soil moisture profiles by an ensemble Kalman filter: Effect of assimilation depth and frequency. Water Resour Res, 43(6).

De Lannoy, G.J.M., Reichle, R.H., Houser, P.R., Pauwels, V.R.N., Verhoest, N.E.C., 2007b. Correcting for forecast bias in soil moisture assimilation with the ensemble Kalman filter. Water Resour Res, 43(9): n/a-n/a.

Dee, D.P., 2005. Bias and data assimilation. Q J Roy Meteor Soc, 131(613): 3323-3343.

Desilets, D., Zreda, M., Ferre, T.P.A., 2010. Nature's neutron probe: Land surface hydrology at an elusive scale with cosmic rays. Water Resour Res, 46(11): W11505.

Entekhabi, D. et al., 2010. The Soil Moisture Active Passive (SMAP) Mission. P Ieee, 98(5): 704-716.

Fereres, E., Soriano, M.A., 2007. Deficit irrigation for reducing agricultural water use. J Exp Bot, 58(2):

147-159.
Franssen, H.J.H. et al., 2011. Operational real-time modeling with ensemble Kalman filter of variably saturated subsurface flow including stream-aquifer interaction and parameter updating. Water Resour Res, 47(2): n/a-n/a.
Franssen, H.J.H., Kinzelbach, W., 2008. Real-time groundwater flow modeling with the Ensemble Kalman Filter: Joint estimation of states and parameters and the filter inbreeding problem. Water Resour Res, 44(9): W09408.
Franz, T.E., Zreda, M., Rosolem, R., Ferre, T.P.A., 2013. A universal calibration function for determination of soil moisture with cosmic-ray neutrons. Hydrology and Earth System Sciences, 17(2): 453-460.
Greybush, S.J., Kalnay, E., Miyoshi, T., Ide, K., Hunt, B.R., 2011. Balance and Ensemble Kalman Filter Localization Techniques. Mon Weather Rev, 139(2): 511-522.
Han, X. et al., 2015a. Correction of systematic model forcing bias of CLM using assimilation of cosmic-ray Neutrons and land surface temperature: a study in the Heihe Catchment, China. Hydrology and Earth System Sciences, 19(1): 615-629.
Han, X., Li, X., Franssen, H.J.H., Vereecken, H., Montzka, C., 2012. Spatial horizontal correlation characteristics in the land data assimilation of soil moisture. Hydrology and Earth System Sciences, 16(5): 1349-1363.
Han, X., Li, X., Rigon, R., Jin, R., Endrizzi, S., 2015b. Soil moisture estimation by assimilating L-band microwave brightness temperature with geostatistics and observation localization. Plos One, 10(1): e0116435.
Han, X.J. et al., 2013. Joint Assimilation of Surface Temperature and L-Band Microwave Brightness Temperature in Land Data Assimilation. Vadose Zone J, 12(3): 0.
Han, X.J., Franssen, H.J.H., Montzka, C., Vereecken, H., 2014a. Soil moisture and soil properties estimation in the Community Land Model with synthetic brightness temperature observations. Water Resour Res, 50(7): 6081-6105.
Han, X.J., Jin, R., Li, X., Wang, S.G., 2014b. Soil Moisture Estimation Using Cosmic-Ray Soil Moisture Sensing at Heterogeneous Farmland. Ieee Geoscience and Remote Sensing Letters, 11(9): 1659-1663.
Harris, F.J., 1978. On the use of windows for harmonic analysis with the discrete Fourier transform. P Ieee, 66(1): 51-83.
Hendrick, L.D., Edge, R.D., 1966. Cosmic-Ray Neutrons near the Earth. Physical Review, 145(4): 1023-1025.
Heng, L.K., Hsiao, T., Evett, S., Howell, T., Steduto, P., 2009. Validating the FAO AquaCrop Model for Irrigated and Water Deficient Field Maize. Agron J, 101(3): 488-498.
Hou, Z.S., Huang, M.Y., Leung, L.R., Lin, G., Ricciuto, D.M., 2012. Sensitivity of surface flux simulations to hydrologic parameters based on an uncertainty quantification framework applied to the Community Land Model. J Geophys Res-Atmos, 117.
Huang, C.L., Li, X., Lu, L., Gu, J., 2008. Experiments of one-dimensional soil moisture assimilation system based on ensemble Kalman filter. Remote Sens Environ, 112(3): 888-900.
Hunt, B.R., Kostelich, E.J., Szunyogh, I., 2007. Efficient data assimilation for spatiotemporal chaos: A local ensemble transform Kalman filter. Physica D: Nonlinear Phenomena, 230(1-2): 112-126.
Jimenez-Bello, M.A., Castel, J.R., Testi, L., Intrigliolo, D.S., 2015. Assessment of a Remote Sensing Energy Balance Methodology (SEBAL) Using Different Interpolation Methods to Determine

872 Evapotranspiration in a Citrus Orchard. Ieee J-Stars, 8(4): 1465-1477.
873 Kerr, Y.H. et al., 2010. The SMOS Mission: New Tool for Monitoring Key Elements ofthe Global Water
874 Cycle. P Ieee, 98(5): 666-687.
875 Kumar, S.V. et al., 2012a. Land surface Verification Toolkit (LVT) – a generalized framework for land
876 surface model evaluation. Geosci Model Dev, 5(3): 869-886.
877 Kumar, S.V. et al., 2012b. A comparison of methods for a priori bias correction in soil moisture data
878 assimilation. Water Resour Res, 48(3): n/a-n/a.
879 Kumar, S.V., Reichle, R.H., Koster, R.D., Crow, W.T., Peters-Lidard, C.D., 2009. Role of Subsurface Physics
880 in the Assimilation of Surface Soil Moisture Observations. J Hydrometeorol, 10(6): 1534-1547.
881 Kurtz, W., Hendricks Franssen, H.J., Kaiser, H.P., Vereecken, H., 2014. Joint assimilation of piezometric
882 heads and groundwater temperatures for improved modeling of river-aquifer interactions.
883 Water Resour Res, 50(2): 1665-1688.
884 Lal, D., Peters, B., 1967. Cosmic Ray Produced Radioactivity on the Earth. In: Sitte, K. (Ed.), Kosmische
885 Strahlung II / Cosmic Rays II. Handbuch der Physik / Encyclopedia of Physics. Springer Berlin
886 Heidelberg, pp. 551-612.
887 Levis, S., Sacks, W.J., 2011. Technical descriptions of the interactive crop management (CLM4CNcrop)
888 and interactive irrigation models in version 4 of the Community Land Model. [Available online
889 at http://www.cesm.ucar.edu/models/cesm1.0/clm/index.shtml.].
890 Li, C., Ren, L., 2011. Estimation of Unsaturated Soil Hydraulic Parameters Using the Ensemble Kalman
891 Filter. Vadose Zone J, 10(4): 1205.
892 Lien, G.Y., Kalnay, E., Miyoshi, T., 2013. Effective assimilation of global precipitation: simulation
893 experiments. Tellus A, 65(0).
894 Liu, Y.Q., Gupta, H.V., 2007. Uncertainty in hydrologic modeling: Toward an integrated data assimilation
895 framework. Water Resour Res, 43(7): n/a-n/a.
896 Merlin, O., Walker, J.P., Panciera, R., Escorihuela, M.J., Jackson, T.J., 2009. Assessing the SMOS Soil
897 Moisture Retrieval Parameters With High-Resolution NAFE'06 Data. Ieee Geoscience and
898 Remote Sensing Letters, 6(4): 635-639.
899 Miyoshi, T., Kondo, K., Imamura, T., 2014. The 10,240-member ensemble Kalman filtering with an
900 intermediate AGCM. Geophys Res Lett, 41(14): 5264-5271.
901 Miyoshi, T., Yamane, S., 2007. Local Ensemble Transform Kalman Filtering with an AGCM at a T159/L48
902 Resolution. Mon Weather Rev, 135(11): 3841-3861.
903 Montzka, C. et al., 2013. Brightness Temperature and Soil Moisture Validation at Different Scales
904 During the SMOS Validation Campaign in the Rur and Erft Catchments, Germany. Ieee T
905 Geosci Remote, 51(3): 1728-1743.
906 Montzka, C. et al., 2011. Hydraulic parameter estimation by remotely-sensed top soil moisture
907 observations with the particle filter. Journal of Hydrology, 399(3-4): 410-421.
908 Moradkhani, H., Hsu, K.-L., Gupta, H., Sorooshian, S., 2005a. Uncertainty assessment of hydrologic
909 model states and parameters: Sequential data assimilation using the particle filter. Water
910 Resour Res, 41(5): n/a-n/a.
911 Moradkhani, H., Sorooshian, S., Gupta, H.V., Houser, P.R., 2005b. Dual state–parameter estimation of
912 hydrological models using ensemble Kalman filter. Adv Water Resour, 28(2): 135-147.
913 Njoku, E.G., Chan, S.K., 2006. Vegetation and surface roughness effects on AMSR-E land observations.
914 Remote Sens Environ, 100(2): 190-199.
915 Oleson, K. et al., 2013. Technical Description of version 4.5 of the Community Land Model (CLM). Ncar

916 Technical Note NCAR/TN-503+STR, National Center for Atmospheric Research, Boulder, CO,
917 422 pp.
918 Park, S.K., Xu, L., 2009. Data assimilation for atmospheric, oceanic and hydrologic applications.
919 Springer, Berlin/Heidelberg, 730 pp.
920 Pauwels, V.R.N. et al., 2009. Optimization of Soil Hydraulic Model Parameters Using Synthetic Aperture
921 Radar Data: An Integrated Multidisciplinary Approach. Ieee T Geosci Remote, 47(2): 455-467.
922 Reichle, R.H., Crow, W.T., Koster, R.D., Sharif, H.O., Mahanama, S.P.P., 2008. Contribution of soil
923 moisture retrievals to land data assimilation products. Geophys Res Lett, 35(1).
924 Reichle, R.H., Kumar, S.V., Mahanama, S.P.P., Koster, R.D., Liu, Q., 2010. Assimilation of
925 Satellite-Derived Skin Temperature Observations into Land Surface Models. J Hydrometeorol,
926 11(5): 1103-1122.
927 Rosolem, R., Gupta, H.V., Shuttleworth, W.J., Zeng, X., de Gonçalves, L.G.G., 2012. A fully
928 multiple-criteria implementation of the Sobol′ method for parameter sensitivity analysis.
929 Journal of Geophysical Research: Atmospheres, 117(D7): D07103.
930 Rosolem, R. et al., 2014. Translating aboveground cosmic-ray neutron intensity to high-frequency soil
931 moisture profiles at sub-kilometer scale. Hydrology and Earth System Sciences, 18(11):
932 4363-4379.
933 Rosolem, R. et al., 2013. The Effect of Atmospheric Water Vapor on Neutron Count in the Cosmic-Ray
934 Soil Moisture Observing System. J Hydrometeorol, 14(5): 1659-1671.
935 Ruiz, J.J., Pulido, M., Miyoshi, T., 2013. Estimating Model Parameters with Ensemble-Based Data
936 Assimilation: A Review. J Meteorol Soc Jpn, 91(2): 79-99.
937 Sampathkumar, T., Pandian, B.J., Mahimairaja, S., 2012. Soil moisture distribution and root characters
938 as influenced by deficit irrigation through drip system in cotton-maize cropping sequence. Agr
939 Water Manage, 103: 43-53.
940 Schöniger, A., Nowak, W., Hendricks Franssen, H.J., 2012. Parameter estimation by ensemble Kalman
941 filters with transformed data: Approach and application to hydraulic tomography. Water
942 Resour Res, 48(4): n/a-n/a.
943 Schwinger, J., Kollet, S.J., Hoppe, C.M., Elbern, H., 2010. Sensitivity of Latent Heat Fluxes to Initial
944 Values and Parameters of a Land-Surface Model. Vadose Zone J, 9(4): 984-1001.
945 Shuttleworth, J., Rosolem, R., Zreda, M., Franz, T.E., 2013. The COsmic-ray Soil Moisture Interaction
946 Code (COSMIC) for use in data assimilation. Hydrology and Earth System Sciences, 17(8):
947 3205-3217.
948 Velikova, V. et al., 2012. The impact of winter flooding with saline water on foliar carbon uptake and
949 the volatile fraction of leaves and fruits of lemon (Citrus×limon) trees. Functional Plant
950 Biology, 39(3): 199.
951 Vrugt, J.A., Diks, C.G.H., Gupta, H.V., Bouten, W., Verstraten, J.M., 2005. Improved treatment of
952 uncertainty in hydrologic modeling: Combining the strengths of global optimization and data
953 assimilation. Water Resour Res, 41(1).
954 Vrugt, J.A., Gupta, H.V., Nuallain, B.O., 2006. Real-time data assimilation for operational ensemble
955 streamflow forecasting. J Hydrometeorol, 7(3): 548-565.
956 Wagener, T., Sivapalan, M., Troch, P., Woods, R., 2007. Catchment Classification and Hydrologic
957 Similarity. Geography Compass, 1(4): 901-931.
958 Walker, J.P., Willgoose, G.R., Kalma, J.D., 2001. One-dimensional soil moisture profile retrieval by
959 assimilation of near-surface observations: a comparison of retrieval algorithms. Adv Water

Resour, 24(6): 631-650.
Waller, J.A., Dance, S.L., Lawless, A.S., Nichols, N.K., Eyre, J.R., 2014. Representativity error for temperature and humidity using the Met Office high-resolution model†. Q J Roy Meteor Soc, 140(681): 1189-1197.
Wanders, N., Bierkens, M.F.P., de Jong, S.M., de Roo, A., Karssenberg, D., 2014. The benefits of using remotely sensed soil moisture in parameter identification of large-scale hydrological models. Water Resour Res, 50(8): 6874-6891.
Welch, B.L., 1947. The Generalization of Students Problem When Several Different Population Variances Are Involved. Biometrika, 34(1-2): 28-35.
Wood, E.F. et al., 2011. Hyperresolution global land surface modeling: Meeting a grand challenge for monitoring Earth's terrestrial water. Water Resour Res, 47(5): W05301.
Wu, C.-C., Margulis, S.A., 2013. Real-Time Soil Moisture and Salinity Profile Estimation Using Assimilation of Embedded Sensor Datastreams. Vadose Zone J, 12(1): 0.
Zeng, X.B., 2001. Global vegetation root distribution for land modeling. J Hydrometeorol, 2(5): 525-530.
Zreda, M., Desilets, D., Ferre, T.P.A., Scott, R.L., 2008. Measuring soil moisture content non-invasively at intermediate spatial scale using cosmic-ray neutrons. Geophys Res Lett, 35(21): L21402.
Zreda, M. et al., 2012. COSMOS: the COsmic-ray Soil Moisture Observing System. Hydrology and Earth System Sciences, 16(11): 4079-4099.

Table List

984 Table 1 Summary of perturbation parameters for atmospheric forcing data

Variables	**Noise**	**Standard deviation**	**Time Correlation scale**	**Forcing Cross Correlation**
Precipitation	Multiplicative	0.5	24 h	[1.0,-0.8, 0.5, 0.0,
Shortwave radiation	Multiplicative	0.3	24 h	-0.8, 1.0,-0.5, 0.4,
Longwave radiation	Additive	20 W/m^2	24 h	0.5, -0.5, 1.0, 0.4,
Air temperature	Additive	1 K	24 h	0.0, 0.4, 0.4, 1.0]

985

986

Figure List

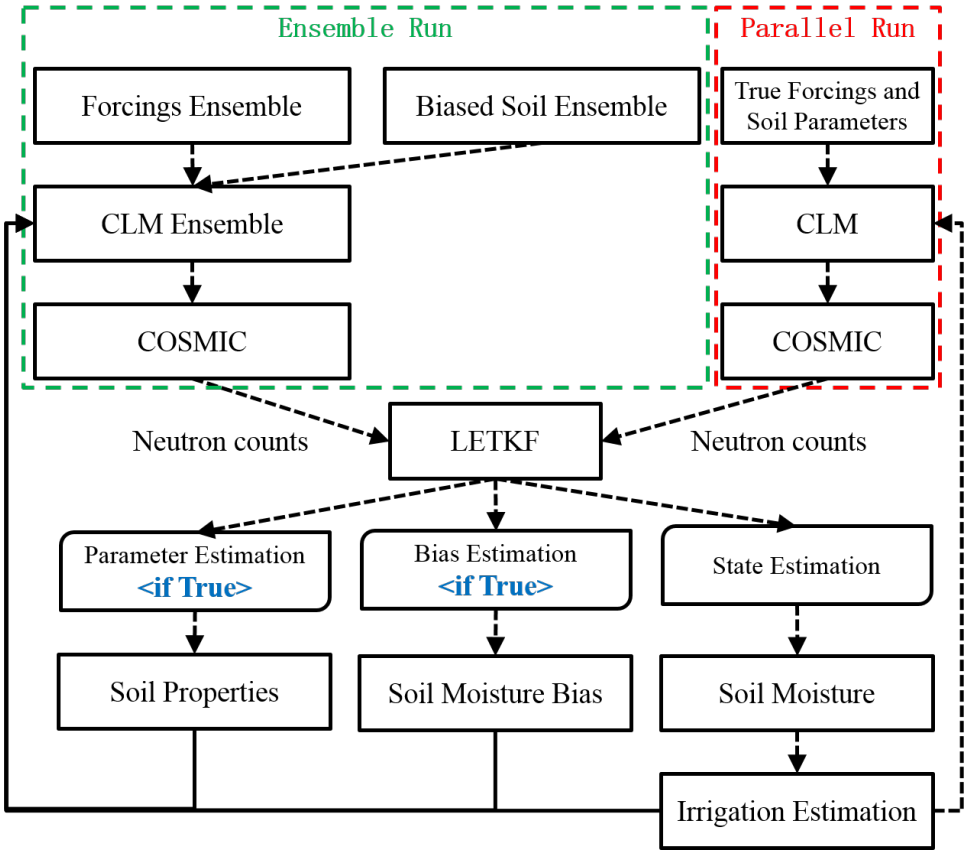

1013

1014 Figure 1. Schematic overview of the different steps of the irrigation optimization

1015 procedure

1016

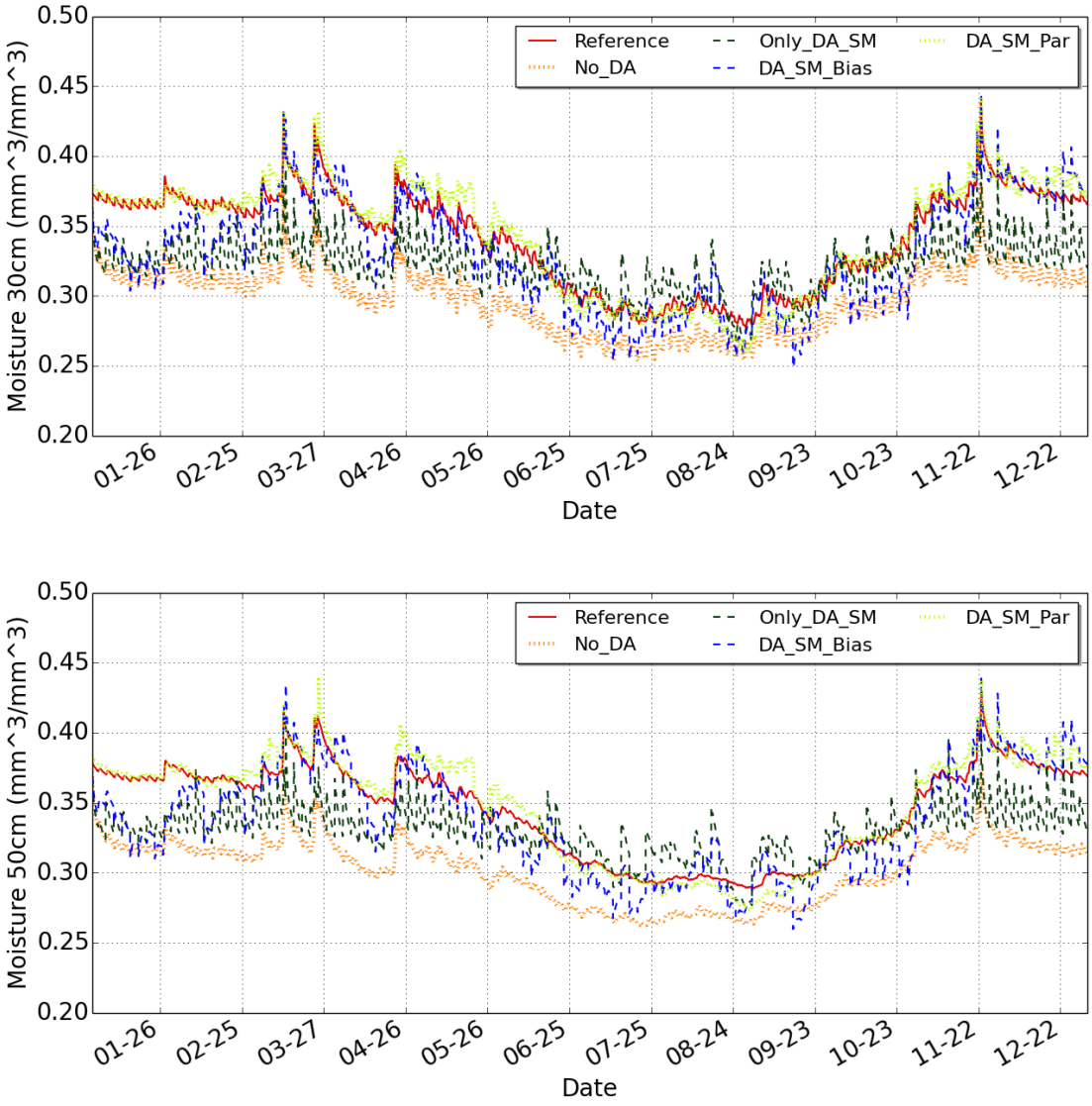

Figure 2. Soil moisture content at 30 cm (upper graph) and 50 cm (lower graph) depth at the CRP location for the different simulation scenarios

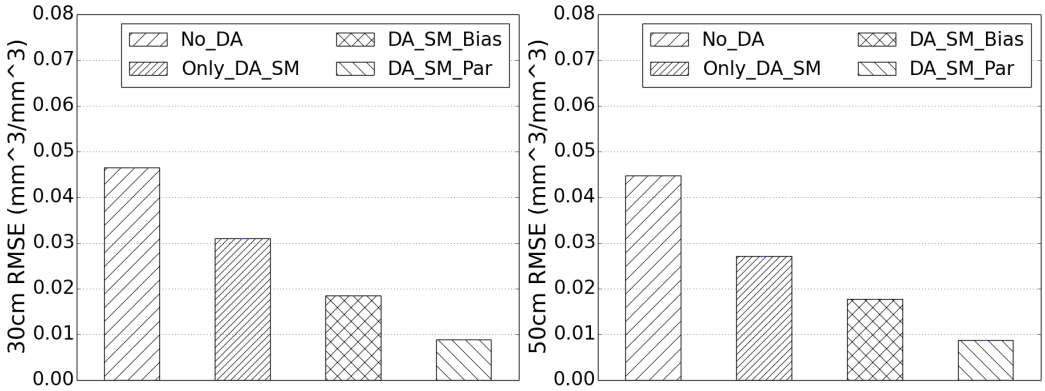

1022

1023 Figure 3. RMSE values for soil moisture content at 30 cm depth (left graph) and 50

1024 cm depth (right graph) for the different scenarios at the CRP location

1025

1026

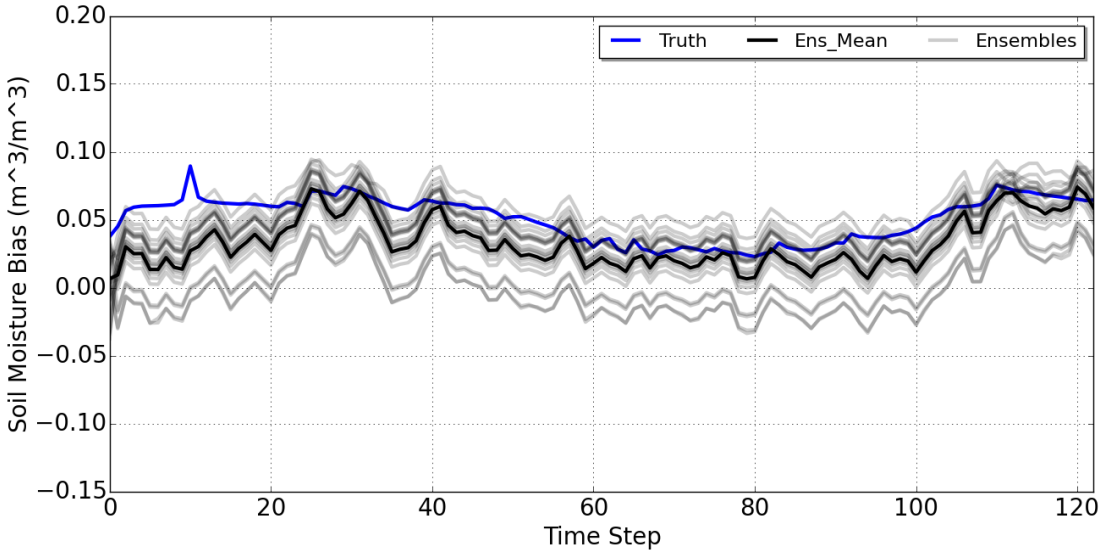

Figure 4. Temporal evolution (collected every three days) of soil moisture bias for the first soil layer at the CRP location (scenario DA_SM_Bias). The true soil moisture bias was calculated from the scenario No_DA and is shown in blue. The unit of x-axis is for time steps of 3 days.

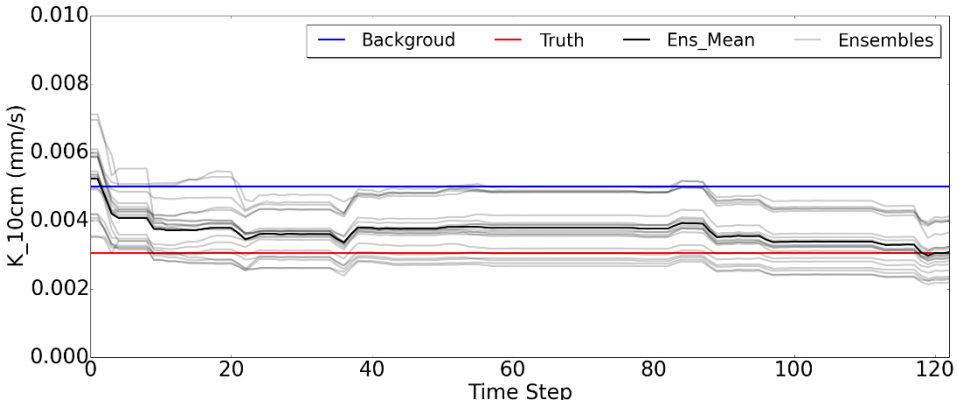

1035

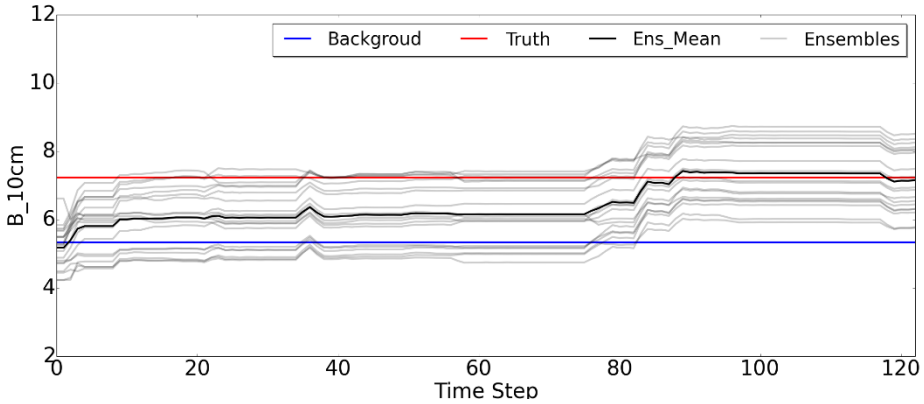

1036

1037 Figure 5. Temporal evolution (collected every three days) of saturated hydraulic
1038 conductivity *K* of soil (K_10cm) and the empirical parameter *B* of the Clapp–
1039 Hornberger parameterization (B_10cm) at the CRP location for the scenario
1040 DA_SM_Par. The unit of x-axis is for time steps of 3 days.
1041

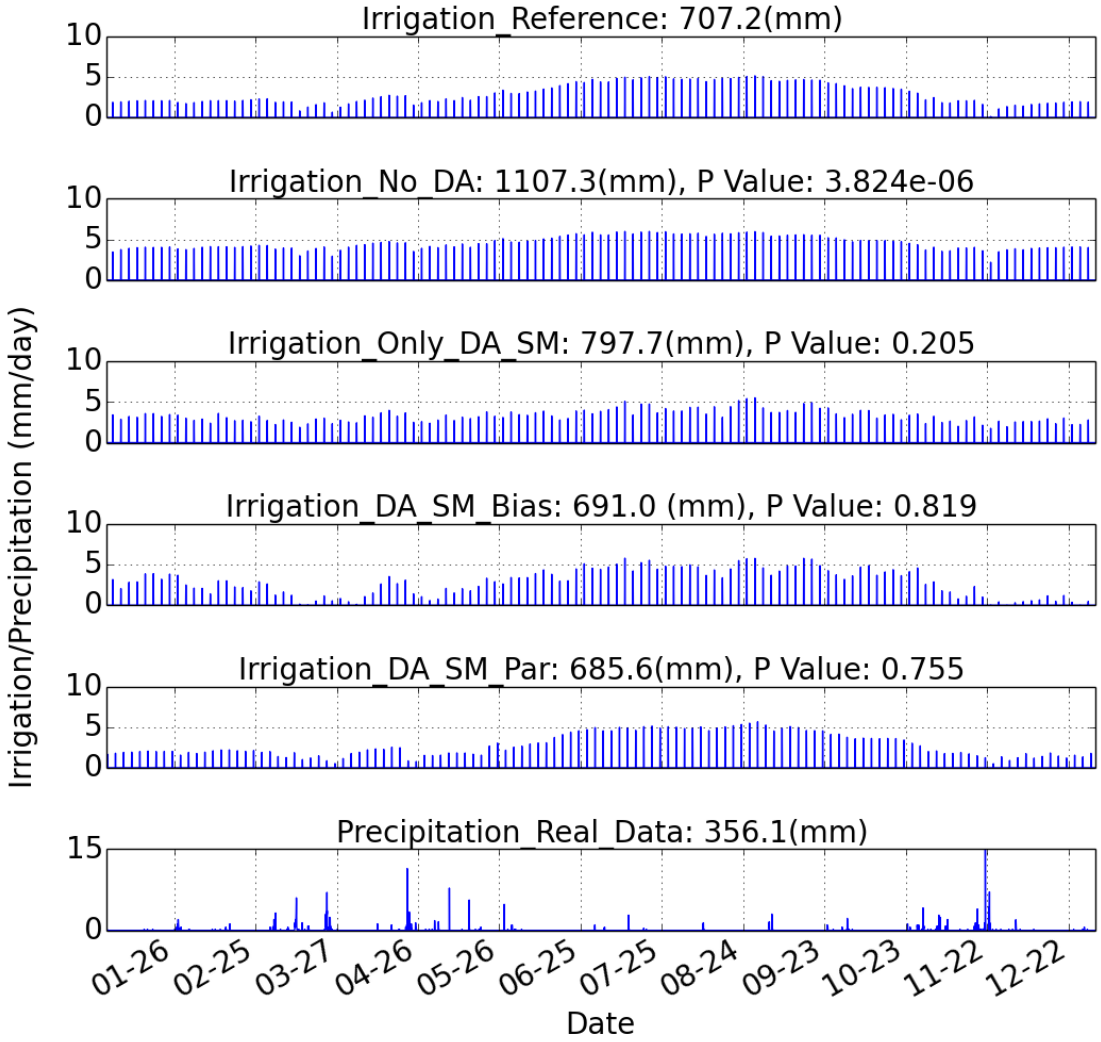

Figure 6. Irrigation requirement as function of time at the CRP location for the different scenarios; t-test statistics (p-value) with significance level 0.05 for comparing the calculated irrigation distribution with reference irrigation are also shown for the different scenarios (large p-values indicate high similarity)

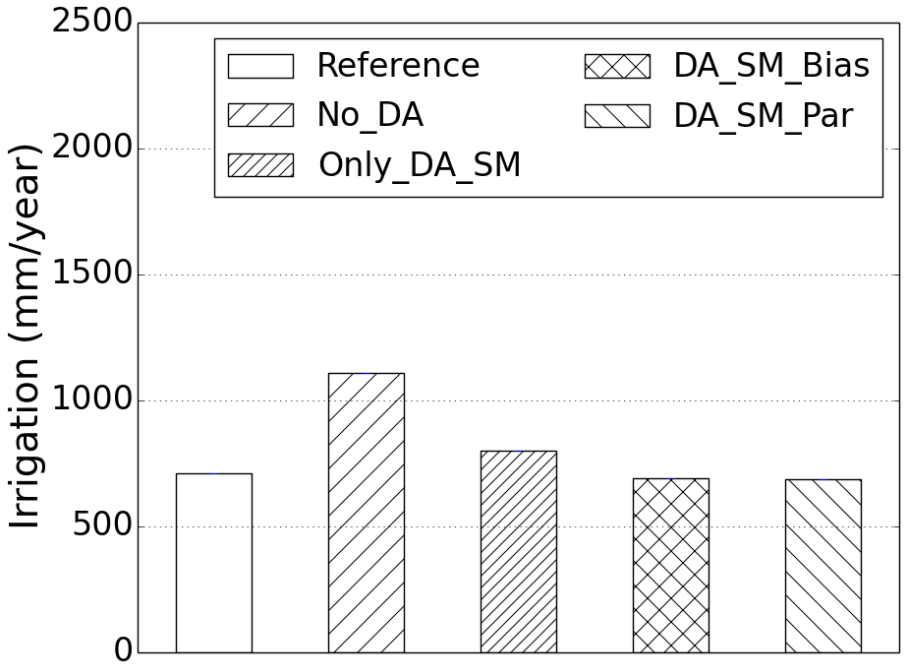

Figure 7. Annual irrigation requirement according to the different scenarios at the CRP location

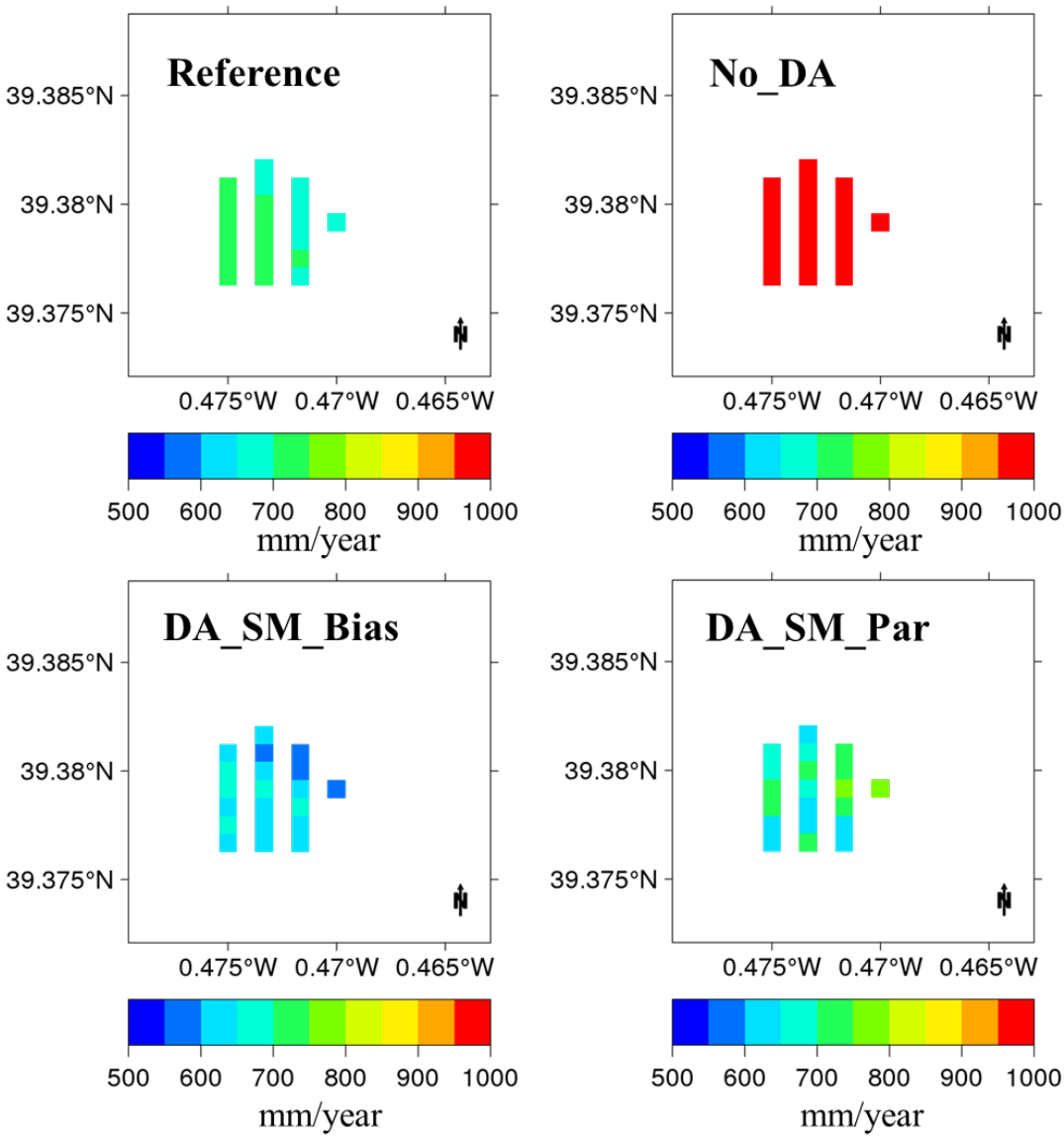

Figure 8. Annual irrigation calculated for different simulations scenarios and compared to the reference scenario

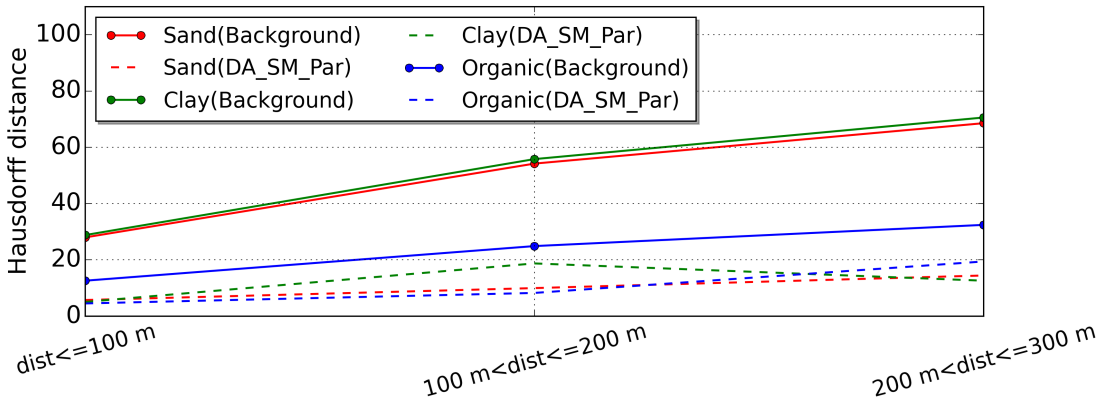

Figure 9. Hausdorff distance values for background soil properties (sand fraction, clay fraction and organic matter density) and estimated soil properties (scenario DA_SM_Par). Results are plotted as function of the distance between model grid cells and the CRP location

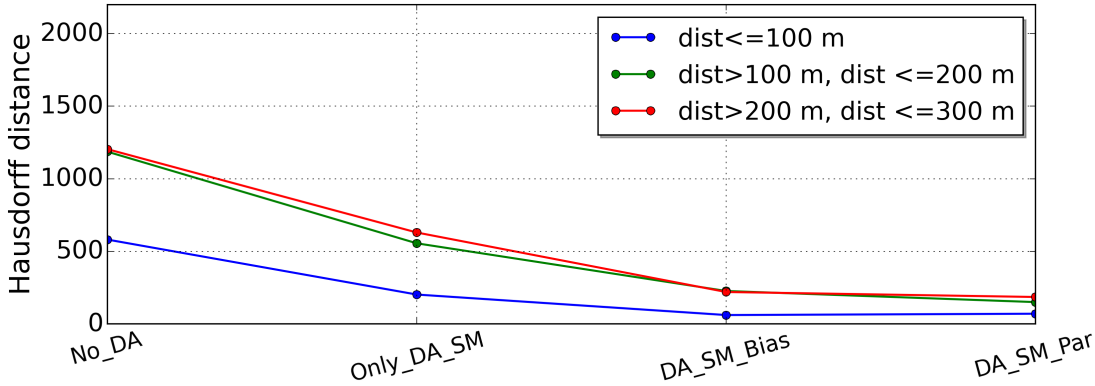

Figure 10. Hausdorff distance values of calculated annual irrigation requirement, compared to reference irrigation, for different scenarios. Results are plotted as function of distance between model grid cells and CRP location